ULF Waves in the Foreshock Around the Moon: Statistical Approach

Anna Salohub[1], Jana Safrankova[2], Zdenek Nemecek[2], Frantisek Nemec[1], and Gilbert Pi[3]

[1]Charles University
[2]Charles University, Faculty of Mathematics and Physics
[3]Charles University in Prague

November 18, 2022

Abstract

A broad statistical study addresses for the first time an evolution of ultra-low frequency (ULF) waves/fluctuations in the terrestrial foreshock around the Moon generated through the interaction between the back-streaming particles reflected from the bow shock and the incoming solar wind. They propagate sunward but are convected by the solar wind flow back toward the bow shock and their amplitudes grow. However, our study shows that waves could be growing as well as decaying towards the bow shock under the quasi-radial interplanetary magnetic field. We demonstrate that the statistically determined growth rate is positive and larger for compressive variations of the density and magnetic field strength than for its components. We show that even if a possible influence of the Moon and its wake is excluded, the growth rate is decreased by non-linear effects leading to saturation of the wave amplitude.

Figure 1.

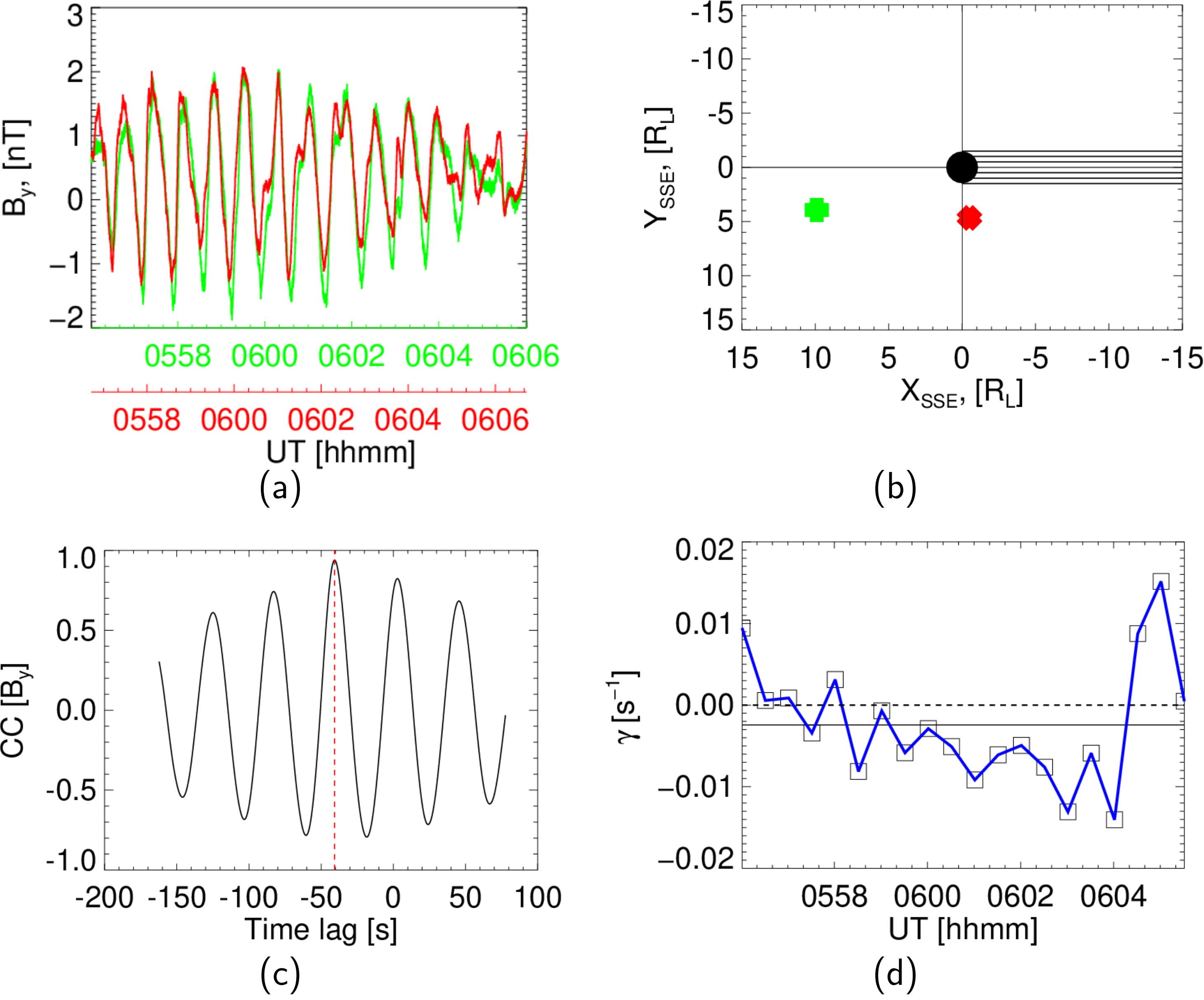

B_y, [nT]
0558 0600 0602 0604 0606
0558 0600 0602 0604 0606
UT [hhmm]
(a)
Y_SSE, [R_L]
X_SSE, [R_L]
(b)
CC [B_y]
Time lag [s]
(c)
γ [s^-1]
UT [hhmm]
0558 0600 0602 0604
(d)

Figure 2.

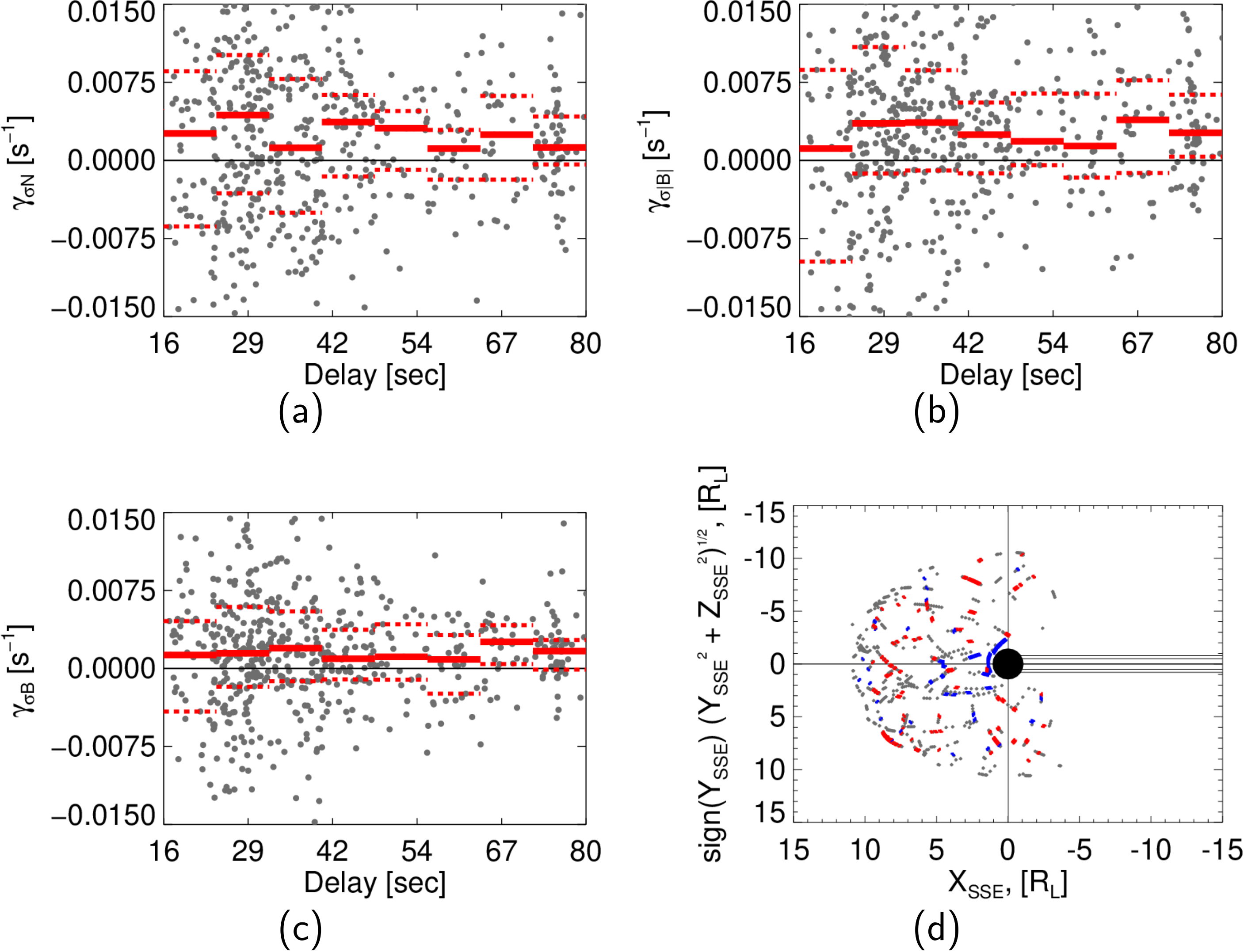

0.0150
0.0075
0.0000
−0.0075
−0.0150
γσN [s−1]
16 29 42 54 67 80
Delay [sec]
(a)
γσ|B| [s−1]
Delay [sec]
(b)
γσB [s−1]
Delay [sec]
(c)
sign(YSSE) (YSSE2 + ZSSE2)1/2, [RL]
XSSE, [RL]
15 10 5 0 -5 -10 -15
(d)

Figure 3.

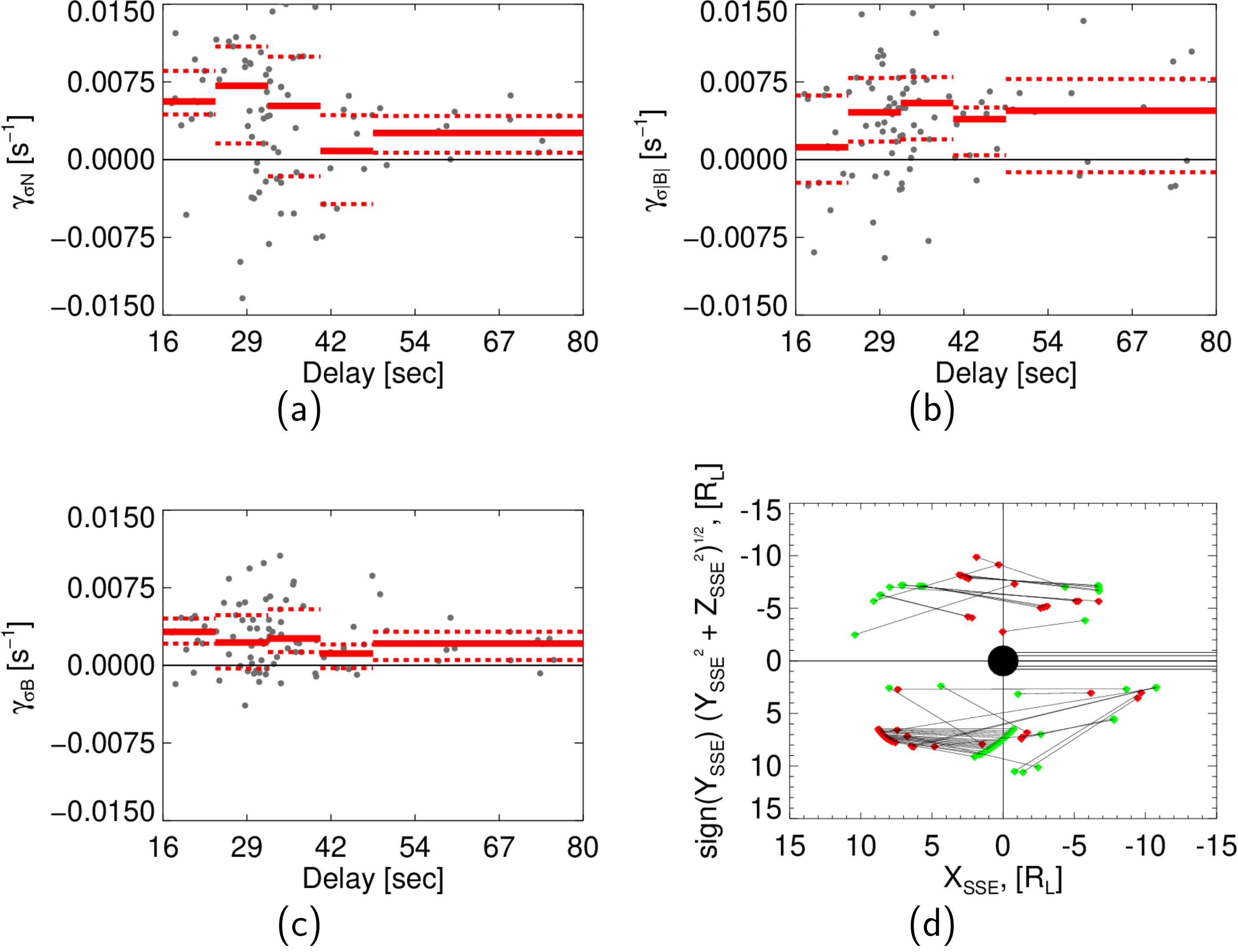

0.0150
0.0075
0.0000
−0.0075
−0.0150
$\gamma_{\sigma N}$ [s^{-1}]
16 29 42 54 67 80
Delay [sec]
(a)
$\gamma_{\sigma|B|}$ [s^{-1}]
Delay [sec]
(b)
$\gamma_{\sigma B}$ [s^{-1}]
Delay [sec]
(c)
sign(Y_{SSE}) (Y_{SSE}^2 + Z_{SSE}^2)$^{1/2}$, [R_L]
-15 -10 -5 0 5 10 15
15 10 5 0 -5 -10 -15
X_{SSE}, [R_L]
(d)

Figure 4.

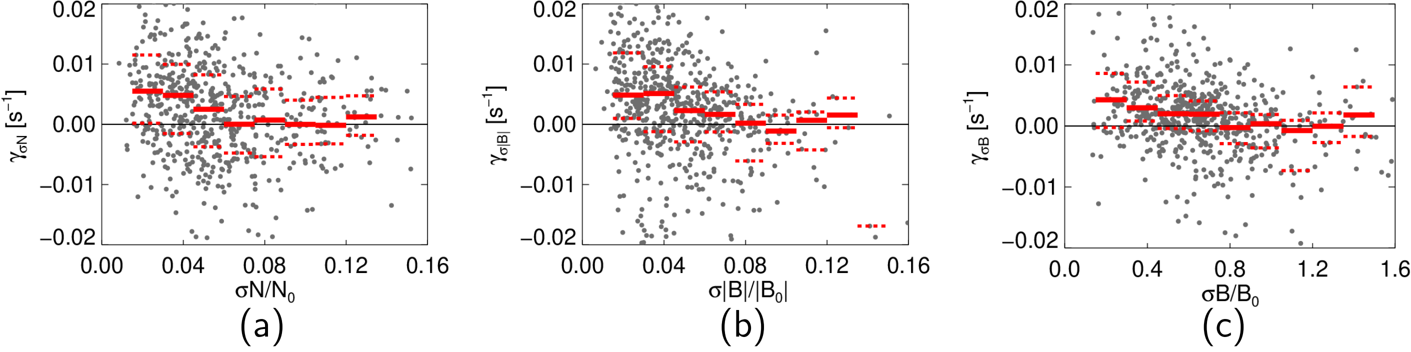

0.02
0.01
0.00
−0.01
−0.02
$\gamma_{\sigma N}$ [s^{-1}]
0.00
0.04
0.08
0.12
0.16
$\sigma N/N_0$
(a)
$\gamma_{\sigma|B|}$ [s^{-1}]
$\sigma|B|/|B_0|$
(b)
$\gamma_{\sigma B}$ [s^{-1}]
0.0
0.4
0.8
1.2
1.6
$\sigma B/B_0$
(c)

ULF Waves in the Foreshock Around the Moon: Statistical Approach

A. Salohub[1], J. Šafránková[1], Z. Němeček[1], F. Němec[1], and G. Pi[1]

[1]Charles University, Faculty of Mathematics and Physics, V Holešovičkách 2, 180 00 Prague 8, Czech Republic

Key Points:

- Ultra-low frequency fluctuations in the foreshock at lunar distances are statistically analyzed for the first time
- Statistically determined growth rate is positive and larger for compressive variations under a radial IMF
- As the wave growth rate can be positive or negative for individual time intervals, effects affecting the growth rate are discussed

Corresponding author: J. Šafránková, `jana.safrankova@mff.cuni.cz`

Abstract

A broad statistical study addresses for the first time an evolution of ultra-low frequency (ULF) waves/fluctuations in the terrestrial foreshock around the Moon generated through the interaction between the back-streaming particles reflected from the bow shock and the incoming solar wind. They propagate sunward but are convected by the solar wind flow back toward the bow shock and their amplitudes grow. However, our study shows that waves could be growing as well as decaying towards the bow shock under the quasi-radial interplanetary magnetic field. We demonstrate that the statistically determined growth rate is positive and larger for compressive variations of the density and magnetic field strength than for its components. We show that even if a possible influence of the Moon and its wake is excluded, the growth rate is decreased by non-linear effects leading to saturation of the wave amplitude.

1 Introduction

Ultra-low frequency (ULF) waves in the frequency range of $0.001 - 0.3$ Hz are a continually present feature of the region upstream of the quasi-parallel shock (Russell et al., 1987; Burgess et al., 2012). At quasi-parallel shocks (characterized by the angle between the upstream magnetic field and bow shock normal, θ_{Bn} smaller than 45°), a portion of the solar wind particles is reflected back into the upstream region forming the foreshock (Hoppe & Russell, 1983; Eastwood et al., 2005) and driving the growth of ULF waves (Wilson III, 2016) traveling upstream. The reflected field-aligned ion beams (Thomsen, 1985; Meziane et al., 2013) are observed for $\theta_{Bn} < 45°$ (Eastwood et al., 2005) and excite waves propagating upstream along the interplanetary magnetic field (IMF). However, these waves need some time to grow toward an observable level, thus they are detected farther downstream in a conjunction with the intermediate distribution (Paschmann et al., 1979). The waves propagate through the regions exhibiting strong density gradients of suprathermal particles, thus they gain a compressive component (Kajdič et al., 2017).

The interaction between the solar wind (SW) and ions reflected at the bow shock has the resonant and non-resonant character and may lead to particle acceleration and plasma heating (Treumann & Pottelette, 2002; Selzer et al., 2014). Instabilities are a primary mechanism exciting transverse waves, propagating mostly parallel and anti-parallel to the IMF. Waves traveling along the ion beam are resonant (Landau resonance), while waves propagating anti-parallel to the beam become unstable in the presence of temperature anisotropy (Sentman et al., 1981; Gary et al., 1998). The excited waves propagate upstream and they are growing but they are convected toward the Earth in the super Alfvénic SW flow (Hoppe et al., 1981; Burgess, 1997), thus the waves of larger amplitudes are observed closer to the bow shock. A presence of waves leads to the SW beam deceleration (Urbář et al., 2019) and deflection (Gutynska et al., 2020).

Simulations (Blanco-Cano et al., 2006; Omidi, 2007; Palmroth et al., 2015) have shown that the foreshock geometry and plasma parameters change with the IMF orientation. Under a nearly radial IMF, the foreshock is permeated by two types of wave modes: the weakly compressive quasi-sinusoidal waves and the magnetosonic compressive fluctuations (Berdichevsky et al., 1999). The weakly compressive waves can propagate at angles up to 30° to the ambient field, in contrast to magnetosonic waves, propagating at larger angles. Weakly compressive waves are dominant far from the bow shock, the second population of ULF fluctuations is observed close to the foreshock edge (Meziane et al., 2004; Palmroth et al., 2015).

Howard et al. (2017) presented a case study of two-point ARTEMIS observations of right-hand polarized ULF waves and reflected SW ions in the lunar environment. The Moon lacks a global magnetic field but it possesses localized crustal magnetic fields (Halekas et al., 2001; Mitchell et al., 2008) and these large-scale magnetic anomalies reflect a part of incoming SW ions before they impact the lunar surface. The reflected ions excite waves that interact with the waves already present in this environment through various mechanisms. Nakagawa et al. (2011, 2012) and Halekas et al. (2013) have reported waves driven by resonant interactions with reflected protons in frequencies ranging from 0.0083 to 10 Hz with both left- and right-hand polarizations in the spacecraft frame. Howard et al. (2020) examined their characteristics and the conditions under which they are likely to occur.

Dorfman et al. (2017) reported the ULF wave growth rate in the foreshock. They applied the data of two ARTEMIS spacecraft orbiting the Moon to characterize reflected ion beams and relatively monochromatic ULF waves. The distance between both spacecraft along the SW flow was $\approx 2.5\,R_E$ (Earth radii) and IMF was nearly radial. They estimated the ULF wave growth rate as 0.010 s^{-1} and the normalized growth rate as $\gamma/\Omega_i \approx 0.035$ (Ω_i is the proton gyroperiod).

Motivated by these investigations, we performed a systematic statistical study focused on conditions under which waves/fluctuations are growing in the lunar surrounding because, according to Jurac and Richardson (2001), the foreshock can extend behind $50\,R_E$ and several events resembling waves of the ion foreshock origin were observed $250\,R_E$ upstream (Berdichevsky et al., 1999). We use observations of two ARTEMIS spacecraft during intervals of a nearly radial IMF when the foreshock occupies a large volume in front of the dayside bow shock. Our analysis is based on standard deviations of the ion density, IMF magnitude and its components computed over 10-minute intervals. We have found that the fluctuation amplitude (standard deviation) of all analyzed quantities can grow but it can be also damped toward the bow shock and we estimate factors influencing the growth rate of ULF fluctuations like spacecraft configurations with respect to the Moon and its wake and permanently changing SW and IMF conditions.

2 Case study

We use the data collected by the twin ARTEMIS probes from 2012 till 2020 years. Probes (referred as THB and THC herein) are in stable equatorial orbits around the Moon with an orbital period of 26 hour. The orbits are highly eccentric with altitudes ranging from $\approx$ 100 to $\approx$ 19.000 km. Two probes move in opposite directions and this allows a large number of different orbital configurations (Angelopoulos, 2008, 2011).

Each spin-stabilized probe carries particle and field instruments. The fluxgate magnetometer provides the magnetic field vector with sampling rate up to 64 Hz (Auster et al., 2008). The electrostatic analyzer (ESA) measures the ion velocity distribution from 1.6 eV to 25 keV (McFadden et al., 2008) with a spin ($\approx$ 3 s) time resolution. We use also data of the solid state telescope (SST) (Angelopoulos, 2008) for monitoring energetic particle fluxes.

In order to demonstrate peculiarities of the wave propagation and amplification, we present one 10-minute subinterval where we apply the similar approach as Dorfman et al. (2017). Variations of the By IMF component for the upstream (green) and downstream (red) spacecraft are shown in Figure 1a for January 16, 2018, 0556 to 0606 UT; Figure 1b presents the mutual position of spacecraft in selenocentric solar ecliptic (SSE) coordinates. Figure 1c shows the cross-correlation of the By components as measured by both spacecraft that peaks at a time lag of -42 s and this lag is also applied in the panel 1a. The value of cross-correlation coefficient ($R = 0.96$) ensures that both spacecraft observe the same wave packet. The ratio of amplitudes determined on 30 s subintervals is then used for a computation of the growth rate. This rate is plotted in Figure 1d as a function of time and one can see that the growth rate is positive at both ends of the studied interval, but it is negative at its center. The average value of the growth rate along this interval is -0.0024 s^{-1} (full horizontal line in Figure 1d), thus the waves are rather decaying in a statistical sense. We should note that the result is qualitatively similar to that shown by Dorfman et al. (2017) in their Figure 3 (panel 3) but our conclusion is that it is difficult to say whether the wave is growing or not. In order to elucidate an evolution of foreshock fluctuations, we perform this extensive study.

3 Selection of data and their processing

The case analysis in the previous section used data transmitted in the ARTEMIS burst mode but such intervals are rare. For this reason, we use data with a spin resolution, thus the study is limited to the frequencies from 0.005 Hz (10-minute interval) to 0.3 Hz (spacecraft spin period). First, we have selected time intervals (with minimum duration of ≈ 30 minutes) of a radial IMF with the cone angle (an angle between the magnetic field vector and Sun-Earth line) lower than 25°. Identified intervals were divided into 10-minute subintervals that are used throughout the study.

We use only data when the Moon is at $X_{GSE} > 30\,R_E$ in the Geocentric Solar Ecliptic (GSE) coordinate system and we rejected data when one of the spacecraft was located in the lunar wake. We defined boundaries of the lunar wake as a prism with dimensions of $-15\,R_L < X_{SSE} < +1\,R_L$; $-1.5\,R_L < Y_{SSE} < +1.5\,R_L$ and $-1.5\,R_L < Z_{SSE} < +1.5\,R_L$ ($R_L \approx 1737$ km, Moon radius). Intervals selected in this way (6128 10-minute subintervals) include different spacecraft configurations around the Moon and its wake.

The above case study uses the correlation for a determination of the time delay between the upstream and downstream spacecraft. However, this approach cannot be applied on the spin resolution data, thus we use a prediction of SW propagation time and calculated as: $\Delta t = (X_{US} - X_{DS})/V_X$, where $(X_{US} - X_{DS})$ is the average distance between the spacecraft along the X_{GSE} axis and V_X is the average SW velocity com-

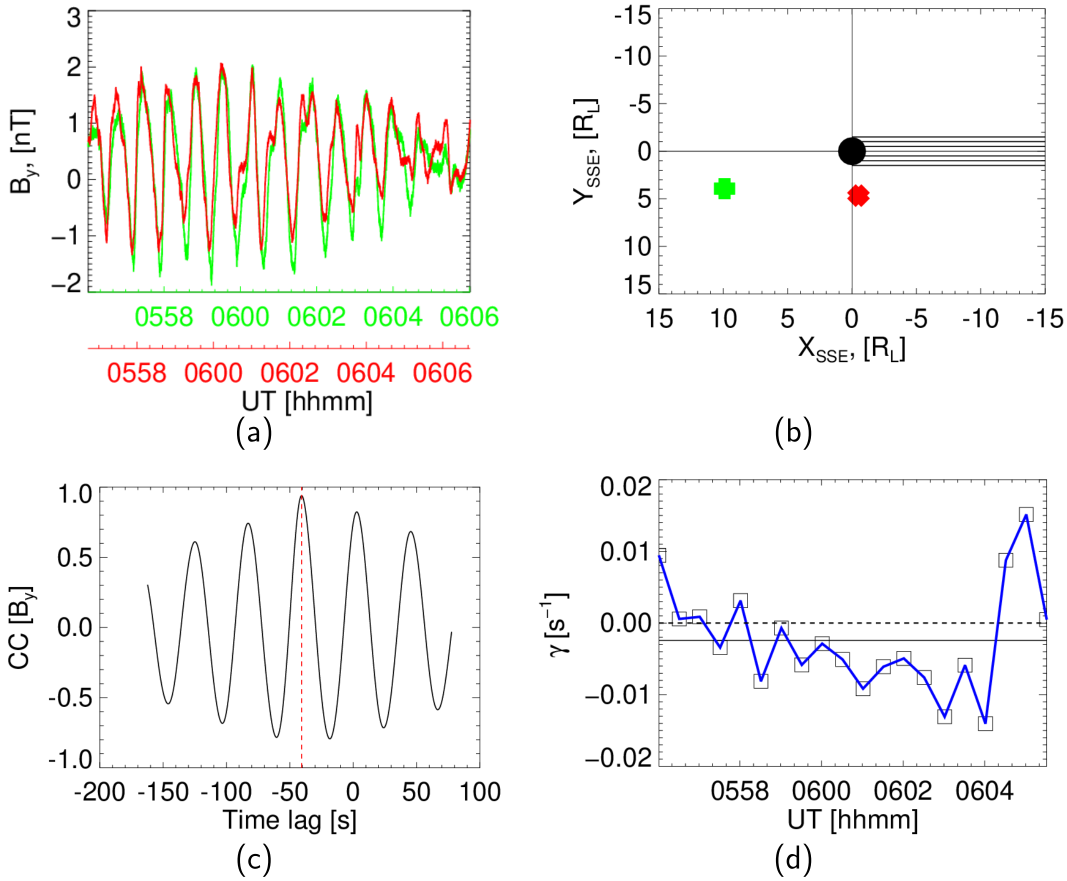

Figure 1. (a) An example of ULF waves observed by THB (red) and THC (green) from 0556 to 0606 UT on January 16, 2018; (b) Locations of THB and THC around the Moon in SSE coordinates; (c) The cross-correlation of the By components as a function of the time lag between both probes; (d) The growth rate γ as a function of time. Note that the black dotted line stands for $\gamma = 0$ and the black full line presents the average value of γ on the whole time interval.

ponent observed by the upstream spacecraft. The propagation times range from a few seconds up to ≈ 80 s.

To be sure that the spacecraft are actually located in the foreshock, we further checked:

1. In SST observations of energetic ions reflected from the bow shock, we use only intervals with the averaged energy flux in the lowest energy channel exceeding 200 keV/(cm^2.s.str.keV) at both probes. This condition reduces our set from 6128 to 3709 intervals.
2. The θ_{Bn} angle at the intersection between the IMF line coming through the spacecraft and the model bow shock (Jeřáb et al., 2005) is lower than 45° and the in-

tersection is closer than -7 R_E. After applying these conditions, we got 1188 data points.

3. We limited the intersection of the IMF line with the model bow shock to $X_{BS} < 25\,R_E$ because the Jeřáb et al. (2005) model can fail in extreme upstream conditions. This particular limit reduces the number of intervals to 1178.
4. Since we investigate the growth rate, we should let the waves a sufficient time to grow and thus we discarded all intervals that did not pass the threshold $X_{US}-X_{DS} > 5\,R_L$. After applying this condition, we obtained 640 data points that represent a basic data subset for the determination of the wave growth rate.

4 Statistical study

We estimate the growth rate, γ using standard deviations computed over 10-minute intervals for the ion density and IMF data. We define it as:

$$\ln \frac{\sigma A_{DS}}{\sigma A_{US}} = \gamma \Delta t \qquad (1)$$

where σA_{DS} and σA_{US} are the standard deviations of variables observed by the downstream and upstream spacecraft, respectively. If $\gamma > 0$, the downstream spacecraft observes the wave amplification whereas $\gamma < 0$ indicates the wave decay. The standard deviations were computed for the IMF magnitude, $\sigma|B|$ and for all components, $\sigma B = (\sigma Bx^2 + \sigma By^2 + \sigma Bz^2)^{1/2}$. Note the difference between $\sigma|B|$ and σB – whereas the former represents the amplitude of a compressive component of fluctuations, the latter rather refers to Alfvénic variations because compressive fluctuation components would be small under the radial IMF orientation (Palmroth et al., 2015). The same procedure was applied for ion density variations, σN.

The resulting growth rates are shown in Figure 2 as a function of the time of solar wind propagation from the upstream to downstream spacecraft (delay = Δt). The gray dots represent values obtained for particular intervals, the red bars stand for median values computed in delay bins and the dashed lines indicate 0.25 and 0.75 quartiles. The growth rates would not depend on the spacecraft separation; the figure demonstrates it in a statistical sense. A detailed examination of Figure 2 reveals that although the fluctuations of all parameters exhibit growing trend in average (the median growth rates are given in Table 1), our set contains a large number of intervals that exhibit wave damping.

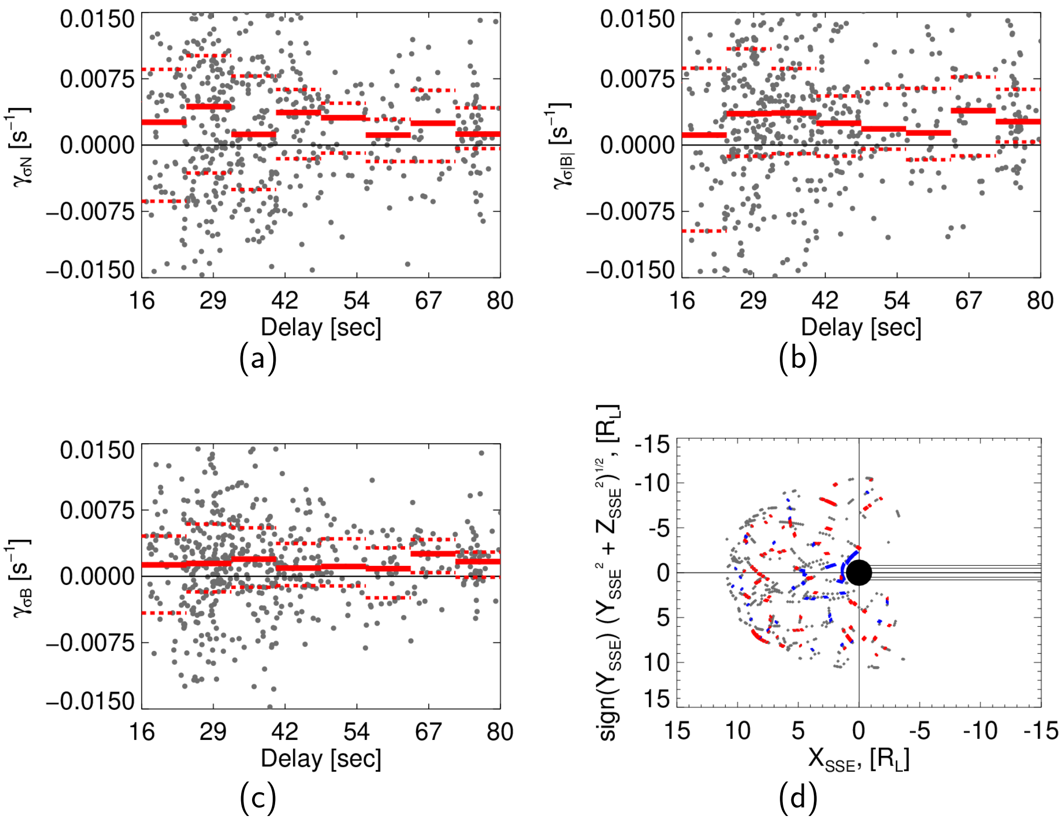

Figure 2. Growth rates of (a) σN; (b) $\sigma|B|$; and (c) σB as a function of the time delay; in all panels, the grey dots (640 data points) represent individual events; the red bars mark the medians in $2\,R_L$ windows; the dashed lines indicate 0.25 and 0.75 quartiles; (d) The locations of the upstream spacecraft in SSE for intervals with growing (red) and damped (blue) waves.

A deeper analysis shows that the criteria used for event selection are too soft and leave a number of events when both spacecraft are still in different environments. Moreover, the situation when we observe positive growth rate in one parameter and negative in other parameters is very frequent. To demonstrate it, we selected events exhibiting positive/negative growth rate in all parameters and plotted the locations of the upstream spacecraft in Figure 2d. Altogether we found 255 events with a positive (red points) and 86 with negative (blue dots) growth rates. The blue dots are concentrated upstream of the Moon or in its vicinity, thus the reflected particles from the lunar surface or from magnetic anomalies (Halekas et al., 2001; Mitchell et al., 2008) can excite new waves and the upstream fluctuations can have larger amplitudes than the original foreshock waves. Under such circumstances, the growth rate computed from the standard deviations could be negative.

Table 1. Median growth rates of σN, $\sigma|B|$, and σB for three sets of the selection criteria (see text for their definition). Note that in the last row, only positive and negative growth rates in all parameters are analyzed.

Conditions	γ_{σ_N}	$\gamma_{\sigma\|B\|}$	$\gamma_{\sigma B}$
Thresholds 1-4 (640 intervals)	0.0030	0.0026	0.0014
Thresholds 1-7 (99 intervals)	0.0057	0.0055	0.0032
Thresholds 1-7 (48 intervals)	0.0077	0.0630	0.0046

Since the analysis of the Moon influence on the foreshock waves is out of the scope of the present study, we applied additional criteria:

5. The angle between average IMF vectors registered by THB and THC is lower than $8°$. This limitation ensures that both spacecraft are magnetically connected to similar points on the bow shock surface; it leaves 517 events from 640.
6. Energetic particle fluxes registered by the first SST energy channel on both probes are similar (their ratio lies in the range of 0.3–9). The range is relatively broad because it should reflect slightly different energy ranges of THB and THC telescopes. This threshold discarded a large number of events; only 362 intervals remain.
7. The line connecting both spacecraft does not cross the Moon or its wake defined above. This threshold is very strong, it leaves only 99 points from the original data set. Among them, 46 events exhibit positive and 2 negative growth rates in all analyzed parameters simultaneously $(\sigma|B|, \sigma N, \sigma B)$.

The growth rate of fluctuations in time intervals passing the above thresholds (99 points) is plotted in Figure 3; Figure 3d shows the locations of both spacecraft connected by thin lines, indicating that the analyzed fluctuations would not be affected by the Moon significantly.

Looking at Figure 3, one note that additional criteria do not change the distribution of growth rates significantly because the spread of individual points is still large, the growth rate varies from -0.005 to $+0.008$. As it can be seen in the second row of Table 1, the median growth rates are by a factor of about 1.4 larger than prior to ap-

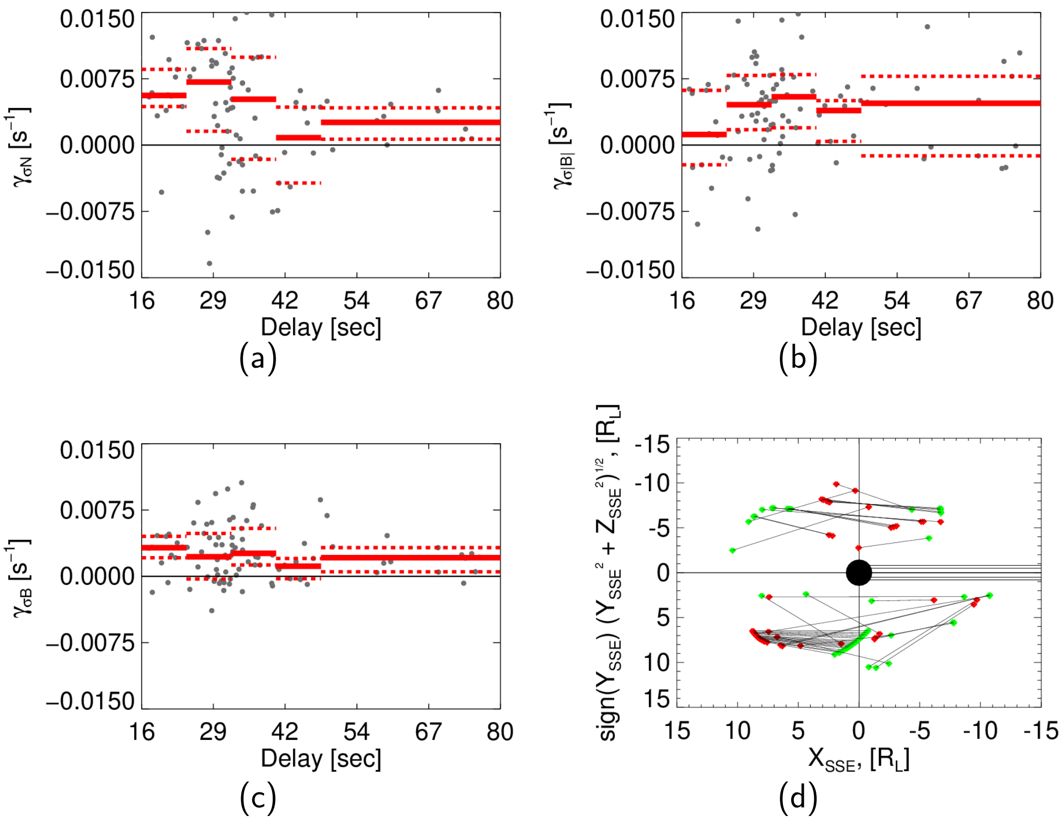

Figure 3. Growth rates of (a) σN; (b) $\sigma|B|$; and (c) σB for 99 points as a function of the time lag in the same format as Fig. 2; (d) The locations of both spacecraft (THB–red and THC–green) for intervals with growing fluctuations (46 events).

plication of criteria 5–7. The last row in Table 1 shows that the medians for the events exhibiting positive or negative growth rates simultaneously for all investigated parameters increase but even this selection does not change their values substantially. If we compare the values in rows, we can note that γ_N and $\gamma_{\sigma|B|}$ are comparable but $\gamma_{\sigma B}$ is by a factor of nearly 2 lower in all sets. We believe that this difference is connected with the character of fluctuations described by these quantities.

5 Discussion

Our statistical analysis demonstrates that close to the Moon ($\approx$ 2–3 R_L), ULF fluctuations are predominantly damped while in a more distant upstream, the waves rather grow. We assume that the reason is that the flux of back streaming ions from the bow shock is shadowed by the Moon (or the lunar wake) and it influences a transfer of energy from particles to waves but this idea should be confirmed by a further investigation. On the other hand, Harada et al. (2015) characterized the large-scale morphology of the region upstream of the Moon and its wake which contains Moon-related particles and waves. SW ions reflected from the unshielded surface and by crustal magnetic fields, together with heavy ions of lunar exospheric origin, are picked up by the solar wind magnetic and electric fields. The authors observed $\approx$ 0.01 Hz and $\approx$ 1 Hz magnetic field fluctuations that partially coincide with populations of the Moon-related ions and found that the morphology of the Moon-related ion and wave distributions is well organized by the upstream magnetic field direction. Our criteria 5–7 would exclude the region potentially influenced by these effects but they still leave intervals exhibiting a negative growth rate. In a follow-up study, we will concentrate on these effects because it is possible that the downstream and upstream spacecraft observe waves of different origin and thus the determination of the growth rate is misleading in such cases.

Depending on the subset used for the growth rate determination, we have found its median value between 0.003 and 0.007 s^{-1} with individual values reaching 0.015 s^{-1}. The median values are a little lower than 0.01 s^{-1} determined in the case study by Dorfman et al. (2017). However, foreshock fluctuations are highly non-linear and thus, there is a question what this growth rate means. Applications of obtained values on the wave growth from the Moon to the subsolar bow shock would lead to a ratio of amplitudes of the order of 20–100 that is unrealistic if the initial fluctuation amplitude in the solar wind is taken into account. The most probable scenario of an evolution of foreshock variations would start with the seed population of turbulent fluctuations that are brought to the outer edge of the foreshock region by the SW flow. The frequency spectrum of such fluctuations is broad and, depending on the instantaneous conditions, a part of this spectrum is amplified. The waves grow but the non-linear effects lead to a saturation of their growth and to excitation of new wave modes. However, new modes are growing at the expense of existing waves and the standard deviations do not increase accordingly. This scenario implies that the initial overall growth rate would be close to the upper limit of rates determined by our study and it would decrease with the fluctuation amplitude. In order to check this idea, we plotted the growth rate as a function of the normalized amplitude of fluctuations of each particular quantity in Figure 4. In order to have sufficient statistics, we use the intervals (640 data points) passing first four thresholds that are used also in Figure 2. Figure 4 shows that the median values of growth rates of all quanti-

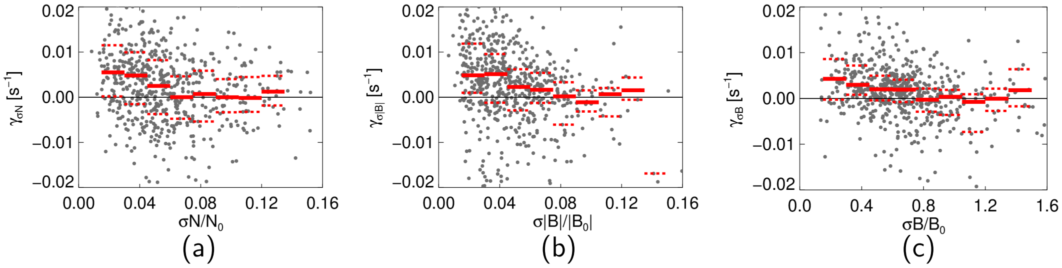

Figure 4. Growth rates of (a) σN; (b) $\sigma|B|$; and (c) σB as a function of the normalized level of fluctuations of a particular quantity (the same description as in Fig. 2).

ties exhibit a clear decreasing trend with an increasing relative fluctuation level that is consistent with our suggestion. We should point out that a saturation of the growth rate can be also seen in Figures 2 and 3 because the medians computed in the time delay bins exhibit a notable decreasing trend, especially for density fluctuations.

Another question is the wave mode which the determined growth rate refers to. We have analyzed fluctuations of the IMF vector, magnitude and ion density. It is expected that the last two parameters are connected with compressive waves whereas the fluctuations of the magnetic field vector describe a level of the weakly compressive Alfvénic component. The previous research revealed that the distant foreshock is predominantly occupied by weakly compressive waves (Meziane et al., 2004; Palmroth et al., 2015), consistently with our observations. Whereas the normalized level of compressive fluctuations $\sigma(|B|/|B_0|)$ does not exceed 0.15, $\sigma(B/|B_0|)$ can reach 1.5 in individual cases. However, dominance of weakly compressive fluctuations is also a typical feature of the SW because a survey of Wind observations at L1 provided median values of $\sigma(|B|/|B_0|) \approx 0.04$ and $\sigma(B/|B_0|) \approx 0.15$. It means that the growth of the non-compressive component starts from a higher level and thus it can reach the saturation level earlier. Other possible explanation can be associated with the suggestion of Kajdič et al. (2017) that the growth of compressive waves requires a sufficient gradient of suprathermal particles, forming deeper in the foreshock. Table 1 shows that the median growth rate of weakly compressive waves, $\gamma_{\sigma B}$ is about one-half of the growth rate of the compressive component in all sets. The question whether these fluctuations grow more slowly or whether they are already close to the saturation level under our conditions cannot be answered by the study that mixes observations at different distance from the foreshock edge.

6 Conclusion

We present a systematic study addressing a behavior of ULF waves in the distant foreshock. Using two-point ARTEMIS observations, we analyze the growth rates of waves under nearly radial IMF computing standard deviations of the IMF magnitude, its components and ion density. Although the fluctuations of all parameters are growing toward the bow shock in a statistical sense, we found also cases exhibiting wave decay. We can conclude that the Moon and its surrounding (wake, particles reflected from the Moon surface) affect the growth rate of waves/fluctuations of foreshock origin significantly and time intervals of foreshock waves should be carefully selected. Such selection allowed us to demonstrate a reduction of the growth rate due to non-linear effects.

Acknowledgments

The authors thank the ARTEMIS working teams for the magnetic field and plasma data that are available online via http://cdaweb.gsfc.nasa.gov/. The present work was supported by the Czech Grant Agency under contract 21-26463S and by Charles University Grant Agency under grant number 1170620.

References

Angelopoulos, V. (2008). The THEMIS mission. *Space Sci. Rev.*, *141*(1), 5-34. doi: 10.1007/s11214-008-9336-1

Angelopoulos, V. (2011). The ARTEMIS mission. *Space Sci. Rev.*, *165*(1), 3-25. doi: 10.1007/s11214-010-9687-2

Auster, H. U., Glassmeier, K. H., Magnes, W., Aydogar, O., Baumjohann, W., Constantinescu, D., ... Wiedemann, M. (2008). The THEMIS fluxgate magnetometer. *Space Sci. Rev.*, *141*(1), 235-264. doi: 10.1007/s11214-008-9365-9

Berdichevsky, D., Thejappa, G., Fitzenreiter, R. J., Lepping, R. L., Yamamoto, T., Kokubun, S., ... Lin, R. P. (1999). Widely spaced wave-particle observations during GEOTAIL and Wind magnetic conjunctions in the Earth's ion foreshock with near-radial interplanetary magnetic field. *J. Geophys. Res. Space Phys.*, *104*(A1), 463-482. doi: 10.1029/1998JA900018

Blanco-Cano, X., Omidi, N., & Russell, C. T. (2006). Macrostructure of collisionless bow shocks: 2. ULF waves in the foreshock and magnetosheath. *J. Geophys. Res.*, *111*(A10). doi: 10.1029/2005JA011421

Burgess, D. (1997). What do we really know about upstream waves? *Adv. Sp. Res.*, *20*(4), 673-682. doi: 10.1016/S0273-1177(97)00455-9

Burgess, D., Möbius, E., & Scholer, M. (2012). Ion acceleration at the Earth's bow shock. *Space Sci. Rev.*, *173*(1), 5-47. doi: 10.1007/s11214-012-9901-5

Dorfman, S., Hietala, H., Astfalk, P., & Angelopoulos, V. (2017). Growth rate measurement of ULF waves in the ion foreshock. *Geophys. Res. Lett.*, *44*, 2120-2128. doi: 10.1002/2017GL072692

Eastwood, J. P., Lucek, E. A., Mazelle, C., Meziane, K., Narita, Y., Pickett, J., & Treumann, R. A. (2005). The foreshock. *Space Sci. Rev.*, *118*(1-4), 41-94. doi: 10.1007/s11214-005-3824-3

Gary, S. P., Li, H., O'Rourke, S., & Winske, D. (1998). Temperature anisotropy and fluctuating field constraints. *J. Geophys. Res.*, *103*, 14.567–14.574.

Gutynska, O., Omidi, N., Sibeck, D. G., Němeček, Z., Šafránková, J., & Lynnyk, A. (2020). Solar wind deflection in the foreshock: Model-data comparison. *J. Geophys. Res. Space Phys.*, *125*(2), e2019JA026970. doi: 10.1029/2019JA026970

Halekas, J. S., Mitchell, D. L., Lin, R. P., Frey, S., Hood, L. L., Acuna, M. H., & Binder, A. B. (2001). Mapping of crustal magnetic anomalies on the lunar near side by the Lunar Prospector electron reflectometer. *J. Geophys. Res.*, *106*, 27,841–27,852. doi: 10.1029/2000JE001380

Halekas, J. S., Poppe, A. R., McFadden, J. P., & Glassmeier, K. H. (2013). The effects of reflected protons on the plasma environment of the Moon for parallel interplanetary magnetic fields. *Geophys. Res. Lett.*, *40*, 4544–4548. doi: 10.1002/grl.50892

Harada, Y., Halekas, J. S., Poppe, A. R., Tsugawa, Y., Kurita, S., & McFadden, J. P. (2015). Statistical characterization of the foremoon particle and wave morphology: ARTEMIS observations. *J. Geophys. Res. Space Phys.*, *120*(6), 4907-4921. doi: 10.1002/2015JA021211

Hoppe, M. M., & Russell, C. T. (1983). Plasma rest frame frequencies and polarizations of the low-frequency upstream waves: ISEE 1 and 2 observations. *J. Geophys. Res.*, *88*(A3), 2021-2027. doi: 10.1029/JA088iA03p02021

Hoppe, M. M., Russell, C. T., Frank, L. A., Eastman, T. E., & Greenstadt, E. W. (1981). Upstream hydromagnetic waves and their association with backstreaming ion populations: ISEE 1 and 2 observations. *J. Geophys. Res.*, *86*(A6), 4471-4492. doi: 10.1029/JA086iA06p04471

Howard, S. K., Halekas, J. S., Farrell, W. M., McFadden, J. P., & Glassmeier, K.-H. (2017). Identifying ultra low frequency waves in the lunar plasma environment using trajectory analysis and resonance conditions. *J. Geophys. Res. Space Phys.*, *122*(10), 9983-9993.

Howard, S. K., Halekas, J. S., Farrell, W. M., McFadden, J. P., & Glassmeier, K.-H. (2020). Solar wind and interplanetary magnetic field influence on ultralow frequency waves and reflected ions near the Moon. *J. Geophys. Res. Space Phys.*, *125*(2), e2019JA027209. doi: 10.1029/2019JA027209

Jeřáb, M., Němeček, Z., Šafránková, J., Jelínek, K., & Měrka, J. (2005). Improved bow shock model with dependence on the IMF strength. *Planet. Space. Sci.*, *53*(1), 85-93. doi: 10.1016/j.pss.2004.09.032

Jurac, S., & Richardson, J. D. (2001). The dependence of plasma and magnetic field correlations in the solar wind on geomagnetic activity. *J. Geophys. Res.*, *106*(A12), 195-205. doi: 10.1029/2000JA000180

Kajdič, P., Blanco-Cano, X., Omidi, N., Rojas-Castillo, D., Sibeck, D. G., & Billingham, L. (2017). Traveling foreshocks and transient foreshock phenomena. *J. Geophys. Res. Space Phys.*, *122*, 9148–9168. doi: 10.1002/2017JA023901

McFadden, J. P., Carlson, C. W., Larson, D., Ludlam, M., Abiad, R., Elliott, B., … Angelopoulos, V. (2008). The THEMIS ESA plasma instrument and in-flight calibration. *Space Sci. Rev.*, *141*(1), 277–302. doi: 10.1007/s11214-008-9440-2

Meziane, K., Hamza, A. M., Wilber, M., Mazelle, C., & Lee, M. A. (2013). On the field-aligned beam thermal energy. *J. Geophys. Res. Space Phys.*, *118*, 6946–6954. doi: 10.1002/2013JA019060

Meziane, K., Mazelle, C., Wilber, M., LeQueau, D., Eastwood, J. P., Reme, H., … Balogh, A. (2004). Bow shock specularly reflected ions in the presence of low-frequency electromagnetic waves: a case study. *Ann. Geophys.*, *22*(7), 2325-2335. doi: 10.5194/angeo-22-2325-2004

Mitchell, D. L., Halekas, J. S., Lin, R. P., Frey, S., Hood, L. L., Acuna, M. H., & Binder, A. (2008). Global mapping of lunar crustal magnetic fields by Lunar Prospector. *Icarus*, *194*, 401-409. doi: 10.1016/j.icarus.2007.10.027

Nakagawa, T., Nakayama, A., Takahashi, F., Tsunakawa, H., Shibuya, H., Shimizu, H., & Matsushima, M. (2012). Large-amplitude monochromatic ULF waves detected by Kaguya at the Moon. *J. Geophys. Res. Space Phys.*, *117*, A04101. doi: 10.1029/2011JA017249

Nakagawa, T., Takahashi, F., Tsunakawa, H., Shibuya, H., Shimizu, H., & Matsushima, M. (2011). Non-monochromatic whistler waves detected by Kaguya on the dayside surface of the Moon. *Earth Planets Space*, *63*(1), 37-46. doi: 10.5047/eps.2010.01.005

Omidi, N. (2007). Formation of cavities in the foreshock. *AIP Conference Proceedings*, *932*(1), 181-190. doi: 10.1063/1.2778962

Palmroth, M., Archer, M., Vainio, R., Hietala, H., Pfau-Kempf, Y., Hoilijoki, S., & et al. (2015). ULF foreshock under radial IMF: THEMIS observations and global kinetic simulation Vlasiator results compared. *J. Geophys. Res. Space Phys.*, *120*(10), 8782-8798. doi: 10.1002/2015JA021526

Paschmann, G., Sckopke, N., Bame, S. J., Asbridge, J. R., Gosling, J. T., Russell, C. T., & Greenstadt, E. W. (1979). Association of low-frequency waves with suprathermal ions in the upstream solar wind. *Geophys. Res. Lett.*, *6*(3), 209-212. doi: 10.1029/GL006i003p00209

Russell, C. T., Luhmann, J. G., Elphic, R. C., Southwood, D. J., Smith, M. F., & Johnstone, A. D. (1987). Upstream waves simultaneously observed by ISEE and UKS. *J. Geophys. Res.*, *92*, 7354-7362. doi: 10.1029/JA092iA07p07354

Selzer, L. A., Hnat, B., Osman, K. T., Nakariakov, V. M., Eastwood, J. P., & Burgess, D. (2014). Temperature anisotropy in the presence of ultra low frequency waves in the terrestrial foreshock. *Astrophys. J. Lett.*, *788*(1), L5. doi: 10.1088/2041-8205/788/1/l5

Sentman, D. D., Edmiston, J. P., & Frank, L. A. (1981). Instabilities of low-frequency parallel propagating electromagnetic waves in the Earth's foreshock region. *J. Geophys. Res. Space Phys.*, *86*(A9), 7487–7497. doi: 10.1029/JA086iA09p07487

Thomsen, M. F. (1985). Upstream suprathermal ions. In B. T. Tsurutani & R. G. Stone (Eds.), *Collisionless Shocks in the Heliosphere: Reviews of Current Research* (p. 253-270). Washington, DC: American Geophysical Union. doi: 10.1029/GM035p0253

Treumann, R. A., & Pottelette, R. (2002). Particle acceleration in the magnetosphere and its immediate environment. *Adv. Sp. Res.*, *30*(7), 1623-1628.

Urbář, J., Němeček, Z., Šafránková, J., & Přech, L. (2019). Solar wind proton deceleration in front of the terrestrial bow shock. *J. Geophys. Res. Space Phys.*, *124*(8), 6553-6565. doi: 10.1029/2019JA026734

Wilson III, L. B. (2016). Low frequency waves at and upstream of collisionless shocks. In A. Keiling, D.-H. Lee, & V. Nakariakov (Eds.), *Low Frequency Waves in Space Plasmas* (Vol. 216, p. 269-291). Washington, DC: American Geophysical Union. doi: 10.1002/9781119055006.ch16